Investigation of Atmospheric Pattern and Simulation of the Frontal Sandstorm Emission over Eastern and Southeastern Iran (case study 23 & 24 April 2019)

Asghari, M.[1], Meshkatee, A.[1*], Ranjbar Saadat Abadi, A.[2] and Moradi, M.[2]

1. Department of Earth Sciences, Islamic Azad University, Science and Research Branch, P.O.Box 14515-775, Tehran, Iran

2. Department of Air Pollution and Atmospheric Chemistry, Atmospheric Science & Meteorogical Research Center, P.O.Box 14965-114, Tehran, Iran

ABSTRACT: The present study simulates the frontal dust storm by means of WRF-Chem model and AFWA emission scheme between April 23 and 24, 2019. It then applies reanalysis data (ERA5) to analyze this case from a synoptic perspective. The simulation results show that the model have been accurately characterized first by the onset of dust from the south-east of the country in Kerman Province and then via its transmission to large areas of the east and south-east. The model output also fits well with satellite images. A quantitative comparison of PM_{10} concentration of the model with actual values shows that the PM_{10} model estimates are larger than actual values, though it predicts the trend of concentration changes well. Examining the synoptic maps, the isobars' curve, wind direction change, and temperature advection in the area reveals the presence of atmospheric fronts within a strong dynamic low-pressure system. This causes high temperature and pressure gradients, in turn speeding up the wind within the region. Results from the synoptic analysis show that by passing the frontal system and behind the cold front, a dust mass is formed, which gradually spreads in eastern and the southeastern regions of Iran. In this case, extreme pressure gradient, cold front passage, low-level jet, wind gust on dry areas of dry Hamoon wetland, and cold air advection over flat area of the Lut Desert are important factors in storm formation and emission, east of the country.

Keywords: frontal dust storm, WRF-Chem, emission, AFWA scheme, southeast.

INTRODUCTION

One of the most abundant airborne particles in the Earth's atmosphere is dust. On a global scale, suspended dust in the Earth's atmosphere is mainly of natural origin (Tegen et al., 2004). In recent years, however, occurrence of widespread and long-term droughts in Western Asia and Middle East, along with the construction of dams in some countries, has increased the frequency and severity of dust storms. The eastern and southeastern parts of Iran are not safe from this phenomenon, which in some cases affects all social and economic activities in the region. In addition to natural factors, human factor, being the main cause of climate change today, has also played a significant role in increasing the concentration of suspended dust in the atmosphere by changing the surface cover (Prospero et al., 2002). Reflecting and absorbing sunlight, dust particles directly influence climate change (Tanaka & Chiba,

2006). They can also indirectly affect the climate through changes in the appearance of clouds and convective activity (Goudie, 2009). Rising dust is a direct consequence of the shear force applied to the earth's surface through air flow, the wind. However, it is necessary to pay attention to the fact that the type of soil, its moisture, and surface cover are effective in how this force affects the process of dust formation. For instance, erosion is more severe in arid and semi-arid areas with slight vegetation.

Responsible for 50% of dust storms in the world, North Africa is the main source of this phenomenon (De Longueville et al., 2010). The Arabian Peninsula comes second in this regard. Due to vast deserts such as the deserts of the Arabian Peninsula, Mesopotamia (the area between Tigris and Euphrates Rivers), the central deserts of Iran as well as Sistan and Baluchestan Region, and the Qaraqum Desert in Turkmenistan, the Middle East, North Africa, and Central Asia are very potential for occurrence of dust storms (Rezazadeh, 2013). Sistan region is one of the most active centers of dust in West Asia (Rashki et al., 2012). Although the areas in which dust is formed are usually arid, semi-arid, and non-vegetated as well as alluvial with fine-grained sediments (Prospero et al., 2002), atmospheric suspended dust could move via atmospheric circulation to areas far beyond its original source of production (Ginoux et al., 2001).

Another study showed that the low-level north-south jet over Afghanistan borderline had a maximum altitude of 300 to 500 meters, with its strongest peak happening in June at a monthly average equal to 20 meters per second. It spread across the border, its presence being essential for emission of dust in this region. Strong ground winds with this low-level jet contribute to dust emission from the Sistan Plain as well as its long-distance transfer (Alizadeh et al., 2014).

Dust storms of April 23 and 24, 2019 in the east and southeast of the country was one of the most widespread dust storms to hit a large part of the country from southwest to southeast. They disrupted land and air traffic in both Kerman and Sistan and Baluchestan Provinces. Given the ongoing socio-economic development programs in the southeastern region of the country and the strategic importance of those programs, it is of particular importance to recognize natural phenomena with the potentials to disrupt socio-economic activities in this region. The present study is, thus, important as it considers the numerous dust storms in Sistan and Baluchestan Region, in the east of the country. It tries to investigate the atmospheric conditions prevailing in frontal dust storms in the east of the country, which though not very frequent, could have many atmospheric hazards when appearing along with the rain.

MATERIAL AND METHODS

In order to investigate the synoptic pattern of dust storms in the east and southeast of Iran, using ECMWF (ERA5) reanalysis data, the study analyzes sea level pressure, geopotential height, wind, temperature, and relative vorticity both at 850 hPa and 500 hPa levels. Related maps are drawn for the peak of the storm time between 23 and 24 April, 2019. The first study, it has considered, is the model of Westphal who presented a practical simulation of soil storms and used a numerical model of multidimensional dust transfer with complete physics, while taking the particle size into account (Westphal et al., 1987; 1988). Due to the importance of the dust phenomenon and its prediction, many operational and research models by different people have been provided (Zakey et al., 2006; Colarco et al., 2009).

In general, three phases of emission, transfer, and deposition are considered for the dust phenomenon. One of the important factors for simulation and prediction of dust concentration in the atmosphere is the

amount of vertical flux of dust from the surface. For this purpose, many schemas have been developed, each utilizing different meteorological quantities and land surface data with different relations to calculate the amount of this flux at network points. Here, in order to simulate the mentioned dust storm in the southeast region numerically, the latest version of the coupled model of Numerical Weather-Atmospheric Prediction-Chemistry (WRF_Chem) has been used. The initial and lateral boundary conditions for the meteorological fields are obtained from the global forecast system (GFS) data with $0.5°$ spatial resolution, available at National Operational Model Archive & Distribution System (http://nomads.ncdc. noaa.gov/).

WRF_Chem is able to model atmospheric chemistry (related to physical meteorology and air pollution), thus it can be used to simulate and predict the concentration of

particulate matter in the atmosphere due to natural mechanisms, human activities (pollutants), and dust in different sizes as well as the way they were transferred and deposited (Grell et al., 2005 and 2011). The model is implemented with two nesting domains with horizontal resolutions of 15 and 5 km. Since the dust particle sizes in the east and southeast are relatively large, the AFWA dust emission scheme has been used in the model to simulate emissions (Kargar et al., 2016). Table 1 shows the other physical schemas, used to implement the model. Output maps of the model were drawn for the second domain. Finally, their accuracy for dust emission was verified by RGB satellite images. Also, the output of PM_{10} concentration of WRF-Chem model was compared and evaluated with PM_{10} measurement data of Zabol Meteorological Center.

Table 1. WRF-Chem physics and chemistry parameterization

Parameterization	Scheme	Namelist variable	Option
Cumulus	Grell 3D	cu_physics	5
Surface model	Noh Land Surface Model (Noh et al., 2003)	sf_surface_physics	2
Surface layer	Monin-Obukhov (Janjic Eta)	sf_sfclay_physics	2
Boundary layer	MYNN 2.5 (Nakanishi and Niino, 2006)	bl_pbl_physics	5
Radiation (SW and LW)	RRTMG (Iacono et al., 2008)	ra_sw(lw)_physics	4
Microphysics	Thompson (Thompson et al., 2008)	mp_physics	8
Chemistry	RADM2	chem_opt	2
Emissions	AFWA	dust_opt	3
Aerosol optics	Maxwell approximation	aer_op_opt	2

The AFWA scheme is based on a modified version of MB95 saltation-based dust emission function. In the AFWA scheme, dust emission is performed as a two-part process, in which large particle saltation is initiated by wind shear and leads to fine particle emissions by bombardment. The scheme is based on the frictional velocity of u_*, the frictional velocity of the static threshold required for the particle entrainment (u_{*t}), the horizontal saltation flux, the resultant bulk vertical dust flux, the particle size distribution of the emitted dust particles, and the size-resolved emitted dust flux. Like GOCART scheme, particles are

divided into a predetermined number of bins based on their effective size. The AFWA scheme uses an independent series of bins for processes based on saltation and emitted dust, representing dust emissions better through saltation bombardment and particle disaggregation (and saving the resources that would have been required to compute advection of saltation particles, which are generally too large for significant long-distance advection) (LeGrand et al., 2019). Tables 2 and 3 present the characteristics, related to nine saltation size bins and five dust size bins in versions 3.8.1 of WRF-Chem, respectively.

It is assumed that all clay particles have a density of 2.5 g/cm³ and all non-clay particles, a density of 2.65 g/cm³, i.e. the density of quartz particles. Finally, the effective diameters, used in the following equations, are assumed to be in centimeter, and for the saltation and dust size bins, they are denoted by the symbols $D_{s,p}$ and $D_{d,p}$ respectively.

Table 2. Saltation particle size bins and their related characteristics, which are in micrometers here, while being in centimeters in the model (Lee Grand et al., 2019)

Saltation size bin (*p*)	Effective diameter ($D_{s,p}$) (µm)	Soil separate class	Soil separate class mass fraction (s_{frac})	Particle density (ρ_p) (g/cm³)
1	1.42	Clay	1	2.50
2	2.74	Silt	0.2	2.65
3	5.26	Silt	0.2	2.65
4	10	Silt	0.2	2.65
5	19	Silt	0.2	2.65
6	36.2	Silt	0.2	2.65
7	69	Sand	0.333	2.65
8	131	Sand	0.333	2.65
9	250	Sand	0.333	2.65

Table 3. Dust particle size bins and their related characteristics, which are in micrometers here, while being in centimeters in the model (Lee Grand et al., 2019).

Dust size bin (*p*)	Lower bound diameter (µm)	Upper bound diameter (µm)	Effective diameter ($D_{d,p}$)(µm)	Particle density (ρ_p)(g/cm³)
1	0.2	2	1.46	2.50
2	2	3.6	2.8	2.65
3	3.6	6	4.8	2.65
4	6	12	9	2.65
5	12	20	16	2.65

The saltation flux is used to calculate dust emission. First, particle-size-dependent saltation fluxes ($H(D_{s,p})$; g/cm s) are calculated following Kawamura (1951):

$$H\left(D_{s,p}\right) = \begin{cases} C_{mb} \dfrac{\rho_a}{g} u_*^3 \left(1 + \dfrac{u_{*t,s,p}}{u_*}\right)\left(1 - \dfrac{u_{*t,s,p}}{u_*^2}\right), & u_* > u_{*t,s,p} \\ 0, & u_* \le u_{*t,s,p} \end{cases} \quad (1)$$

Where C_{mb} is an empirical proportionality constant set to 1.0. The H ($D_{s,p}$) values are then integrated over particle sizes to obtain the total stream-wise horizontal saltation flux (*G*). Estimated contributions of each saltation size bin to total saltation flux (*G*) depend on the surficial coverage of particles in each saltation particle size bin as a fraction of the total surface area of the soil bed. As with common land surface modelling practices (e.g., Mitchell, 2005; W. Wang et al., 2017), the AFWA scheme assumes that all particles comprising the soil column belong to one of three US Department of Agriculture (USDA) defined soil separate categories, based on particle size: sand (50 to 2000 µm), silt (2 to 50 µm), or clay (≤ 2 µm). Instead of the fixed soil separate fractions, used in the GOCART-WRF scheme, the makeup of the soil in the AFWA scheme is set using the soil particle size information for the surface layer of soil (0–30 cm) originally derived from the global FAO-SMW soil dataset by Reynolds et al. (2000).

In order to study the pattern, governing the frontal storms, the maps were drawn at the time of the storm. Figure 1a illustrates the pattern of sea level pressure on April 23, 2019. According to this figure, there is a low-pressure system with a central

pressure of less than 997.5 hPa in eastern part of Iran. One of the troughs of this low pressure has been extended to the southeast of Iran, while the other have spread to the northwest and northeast of Iran. In this figure, a high-pressure system with a central pressure greater than 1027.25 hPa is located on the north side of the Black Sea.

With the expansion of the high pressure of the northern Caspian Sea and its tongue's penetration into the northern strip, a strong pressure gradient has been created, especially at the center of Iran.

Calculations showed that for every 10 degrees of latitude, 12 hPa of pressure

dropped in the eastern and southeastern regions of Iran. Along with this dynamic low pressure, cold, hot and closed fronts got created. Figure 1b shows the sea level pressure for the 24th day of April. High pressure, while getting stronger, had more influence on Iran, causing the east to move towards low pressure and its establishment in Afghanistan.

This trend continued in the following hours, leading to the formation of high pressure with a closed center of more than 1027.25 hPa on the northern part of Iran, and the front related to this system passing through eastern Iran.
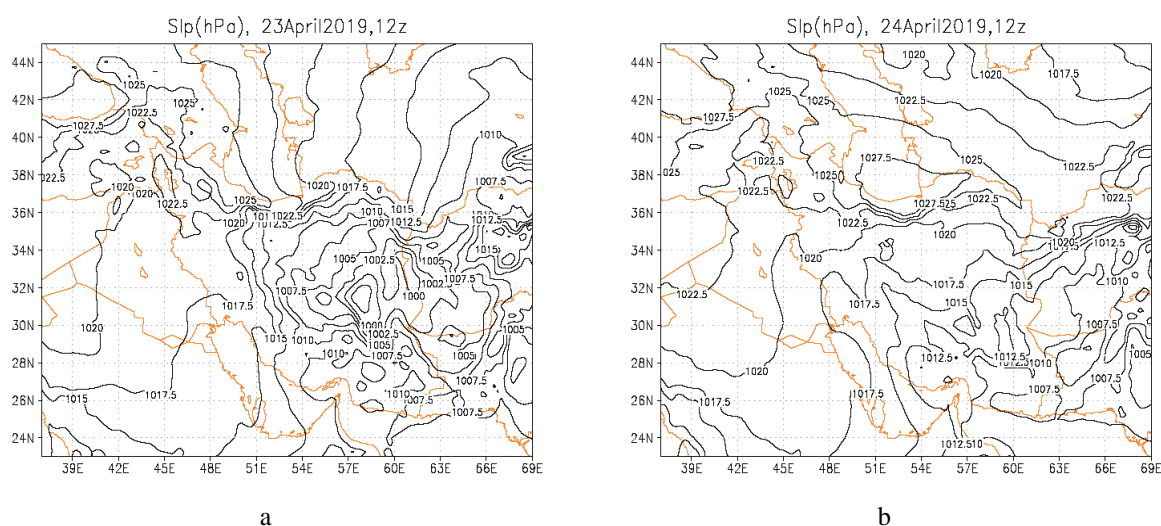

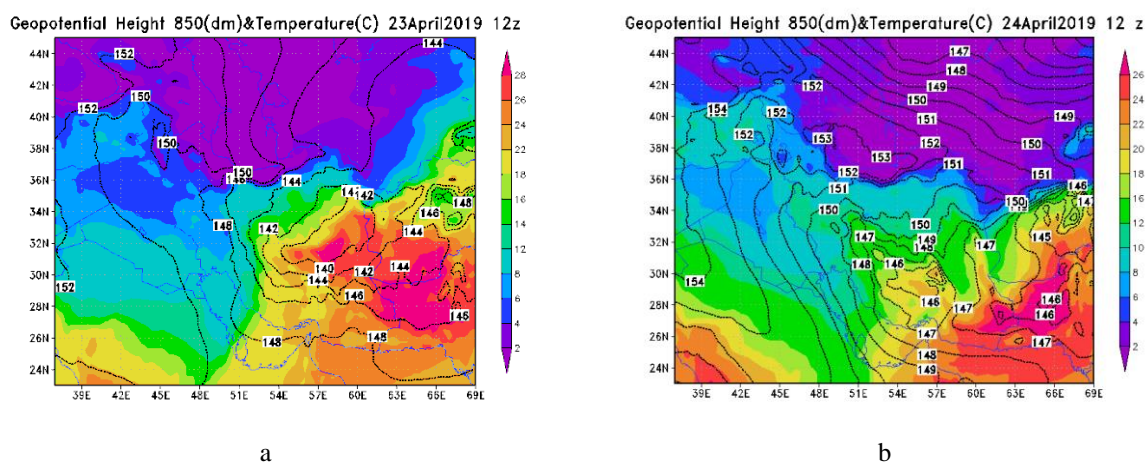**Fig.1. Sea level pressure (hPa), a: 12UTC, 23, b: 12 UTC 12, 24April 2019**

Fig. 2. Geopotential height pattern, wind in meters per second, and temperature in degrees Celsius at 850 hPa, a: 12 UTC, 23 April, b: 12 UTC, 24 April, 2019

West and northwest winds on the central areas, especially Yazd, behind the cold front caused the formation of post-frontal dust and southeast winds in Kerman, South Khorasan, and Sistan and Baluchestan, in turn leading to the formation of frontal dust (Figures 2a and 2b). As the cold front entered, rainfall was reported in several stations of Kerman (Lalehzar 30 mm), South Khorasan (Birjand 5 mm), Sistan and Baluchestan (Zahak 4 mm), and Yazd (Sabzdasht 7 mm) Provinces. Figure 3 demonstrates the total rainfall of stations in each province from April 22 to April 25.

Figure 2a shows the geopotential height, temperature, and wind level of 850 hPa on April 23. According to sea level pressure forms, the cyclone center was located in eastern Iran with a closed center of less than 1400 geopotential meters. The anticyclone center was also formed over the Black Sea. In this figure, the significant change in wind direction and temperature gradient (around latitude 32 degrees) indicates the frontal zone. On April 24 (Figure 2b), the low moved east. The anticyclone intensified, causing more penetration into northern Iran.

Fig. 3. Total rainfall (mm) of each province from of April 22 to April 25, 2019

formed since April 23 in the afternoon and continued until April 24 during the passage of the trough and the cold front through the eastern parts of the country. The intensity of the dust storm, estimated based on the magnitude of the wind speed and the amount of horizontal visibility, was after the passage of the cold front. Table 1 shows the horizontal visibility and wind speed at meteorological stations in the study area. From this table, the horizontal visibility in some stations reached less than 1000 meters and the wind speed reached more than 20 m/s. After crossing the front, the intensity of the storm lessened. Since the end of the 24th day, the dynamic cyclone gradually weakened. Investigations showed that on the 23th day (Figure 3a) with a positive relative vorticity penetration of 500 hPa with

Figures 5a and 5b show the vertical profile of the horizontal wind and the meridional component of the wind from the earth's surface to the upper atmosphere in a 32-degree latitude. The former illustrates the change in wind direction (negative of the meridional component of the wind) from northwest to southeast and its intensification. This change of direction indicates the passage of the trough and the front area. According to Figure 5a, the polar jet passage is visible at higher levels. As the instability intensified on 24 April, the polar jet penetrated lower levels (Figure 5b). At the mid-atmosphere (500 hPa), the active cyclone penetrated from the north, with relatively positive and noticeable vorticity and accompanied by a 24 °C isotherm. Also, the trough moved east (Figure 4a and 4b). The dust was

and complete penetration of the trough and by front crossing on the 24th day of April, the dust storm of the front reached its peak.

values greater than 10×10^{-5} (1/s) to the east of the country, the dust began and with an increase in positive relative vorticity
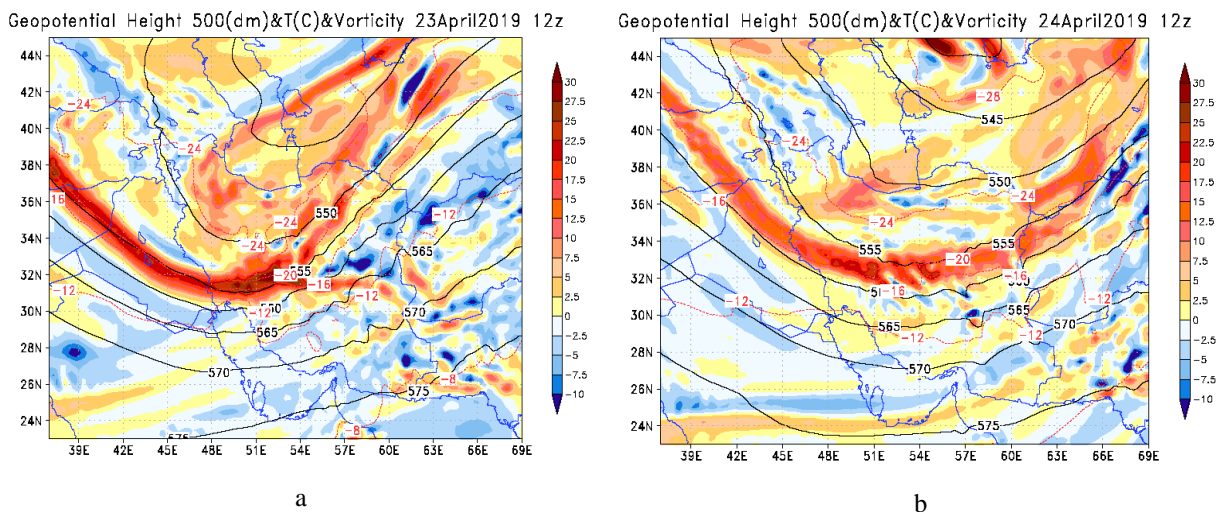

Fig. 4. Geopotential height in terms of geopotential meters, temperature in degrees Celsius and relative vorticity in terms of $\times 10^{-5}$ (1/s) 500 hPa, a: 12 UTC, April 23, b: 12 UTC, April 24, 2019

Table 4. Direction (Degree) and Speed (m/s) of Maximum Wind South East from 22 to 25 April

Maximum wind speed				
Yazd	**Hormozgan**	**South Khorasan**	**Kerman**	**Sistan va Baluchestan**
Gariz 22 m/s 250°	Qeshm 16 m/s 240°	Zohan 23 m/s 160°	Kerman 22 m/s 260°	Saravan 22 m/s 240°
Yazd 19 m/s 240°		Ferdows 16 m/s 310°	Sirjan 19 m/s 210°	
Abar kooh 17 m/s 240°	Kish 15 m/s 300°			Zabol 21 m/s 250°
Marvast 15 m/s 210°		Tabas 15 m/s 300°	Rafsanjan 18 m/s 250°	Kash m/s 19 290°
Meybod 15 m/s 210°				Zahedan 17 m/s 250°

Figures 5a and B show the vertical profile of the horizontal wind and the meridional component of the wind from surface level to the upper atmosphere in a 32-degree latitude. Figure 5a shows the change in wind direction (negative of the meridional component of the wind) from northwest to southeast and its intensification. This change of direction indicates the trough along with the frontal system. According to Figure 5a, the polar jet passage is formed at higher levels. As

the instability did intensify on April 24, the polar jet penetrated to the lower levels (Figure 5b).

Figures 6a and b demonstrate the wind meridian component for April 23 and 24, 2019 in the 30° latitude around Lut Desert. According to these figures, on April 23, a strong wind core (low level jet) formed from the level of 900 to 850 hPa and for the 24th day, with the intensity of the storm, it got strengthened and expanded.
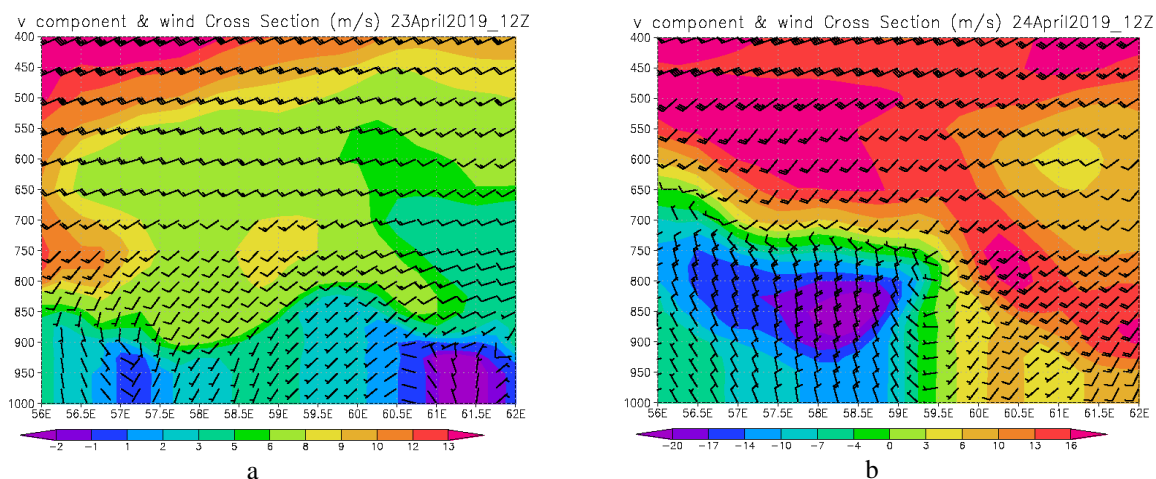
Fig. 5. Vertical profile of wind and its meridional component in meters per second along the latitude of 32 degrees and its meridional component, a: 23, b: April 24, 201.
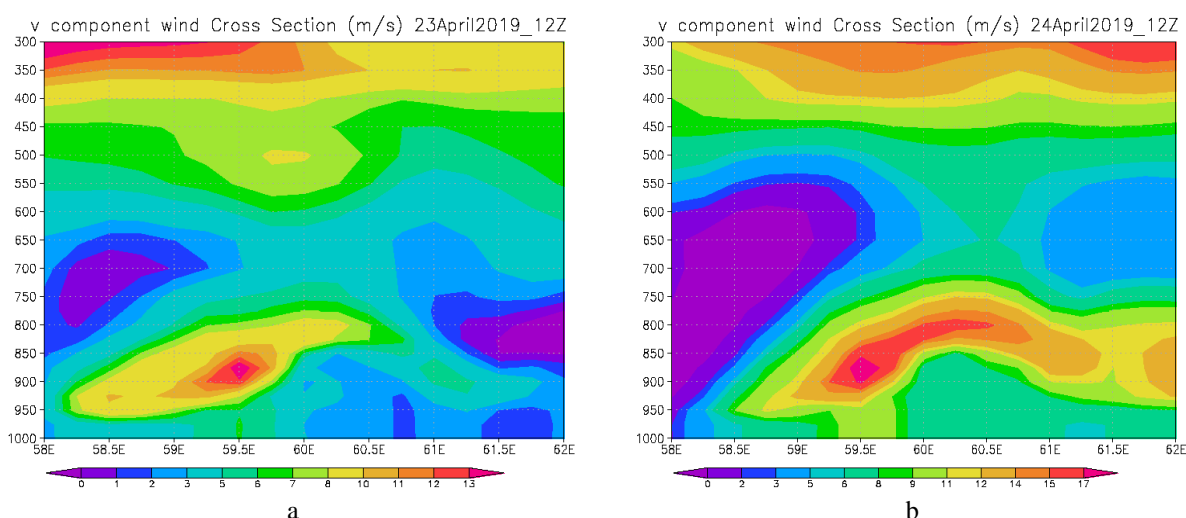

Fig. 6. Vertical profile of meridian component of wind in meters per second, a: 23 b: April 24 in 30 degree orbit (Lut desert)

Figures 7 and 8 show the output of the WRF-Chem model in terms of dust load quantities and PM_{10} concentrations on 23rd and 24th of April, 2019, respectively. The results indicate that dust emission started in the beginning of April 23 from Fahraj and Regan areas (Kerman), its concentration and extent having gradually increased. From the middle of April 23, the dust mass reached the main central and northern regions of Sistan and Baluchestan Province (Zahak, Zabol) as well as some areas in Kerman Province (Kahnooj and Jiroft) and during the 24th day, the dust mass spread out to the front and got covered with clouds. The east of the country and the Zabol region can be seen in the north of Sistan and Baluchestan. This is also confirmed by satellite images. Therefore, in this case, the model simulates the dust spring and its transfer to the east and southeast of the country quite well.

The simulation results show that from the afternoon of the 23rd day, the amount of dust load on the north of Sistan and Baluchestan, especially Zabol, experienced a significant increase (Code 07) caused by the area within the region. For this reason, the highest concentration of dust particles occurred in the early hours of April 24.
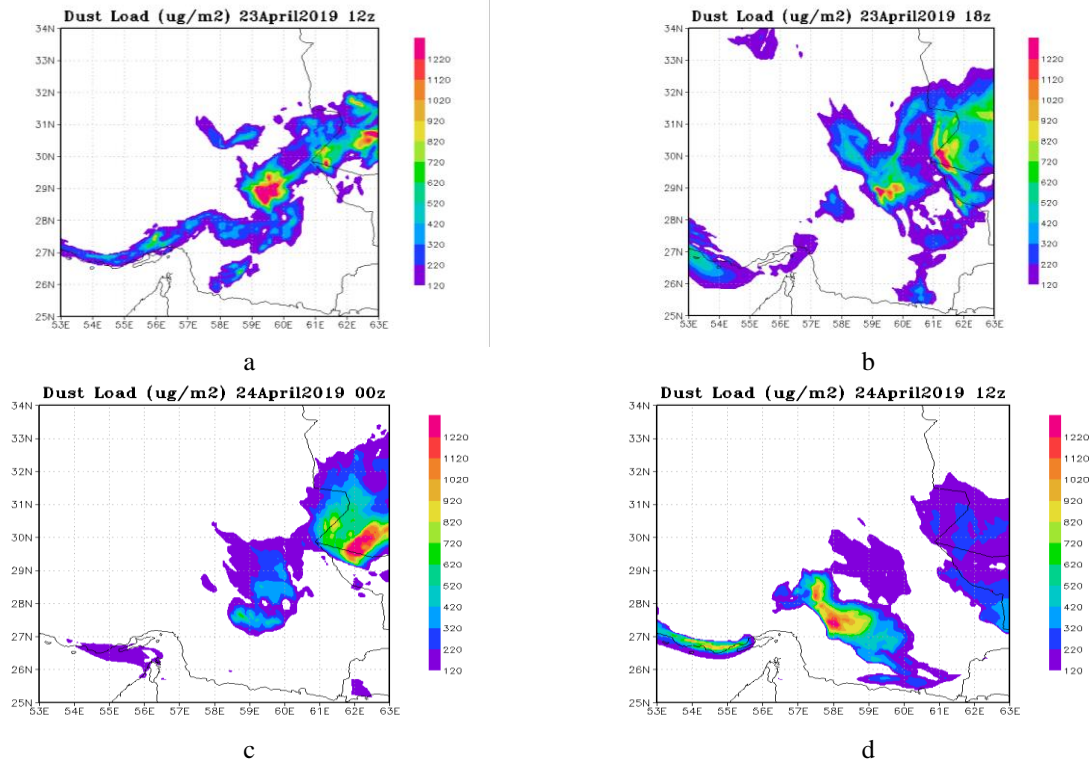
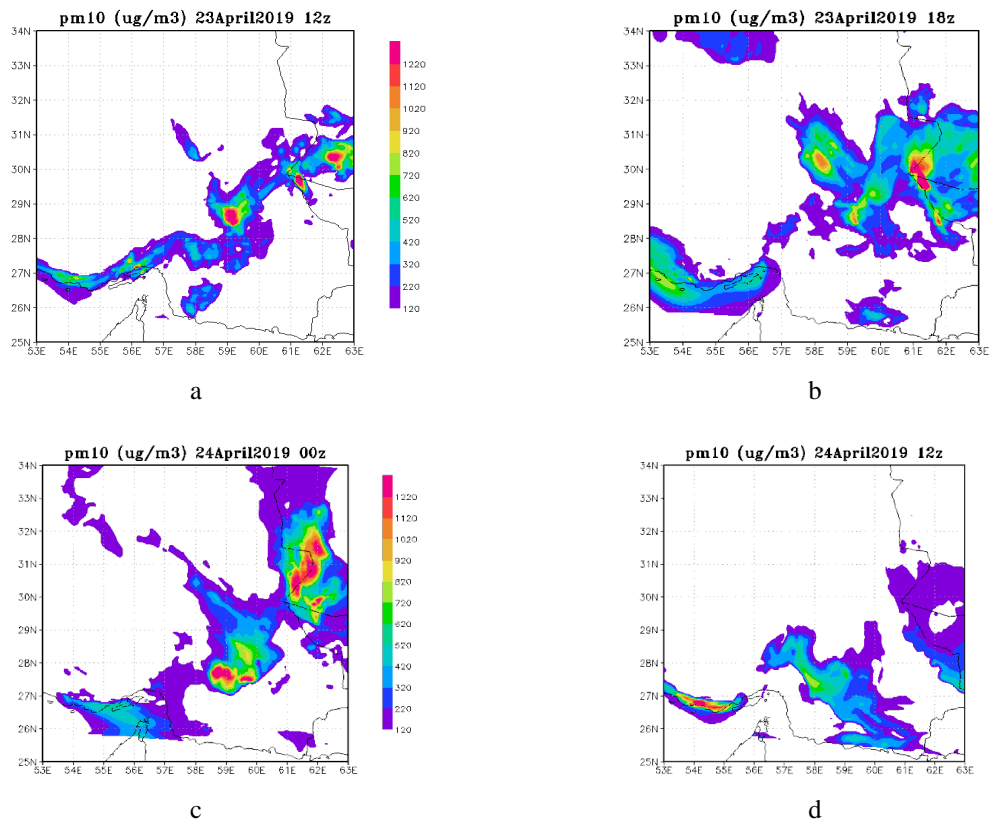**Fig. 7. Dust load (µg/m^3) of AFWA emission scheme output, WRF-Chem model on a, b: 23 and c, d: April 24, 2019**

Fig. 8. PM$_{10}$ Concentration (µg/m^3) of AFWA emission scheme, WRF-Chem model on a, b: 23 and c, d: April 24, 2019

Examining Meteosat Second Generation (MSG) RGB images during the days of the storm showed the advance of dust on the eastern and southeastern regions of Iran along with the emergence of ridge clouds, indicating the passage of the cold front through the region (Figure 9a and 9b). By post-processing the model output and production of PM_{10} particle concentration and dust load maps, areas of the simulation field with maximum particle concentrations (Fahraj and Reagan in the southeast of Kerman Province on the border of Sistan and Baluchestan) can be used as the main sources of dust particle emission. The increase in PM_{10} values as a quantity indicating the dust particle concentration of Zabol station was also consistent with the model outputs, showing that the AFWA scheme performed well in simulating the change process and the maximum dust concentration.

In satellite images, the position of cold and warm fronts and warm air advection in the front of the warm front and cold air advection showed that the dust storm was located behind the cold front as a post-frontal system. The cold front accompanied and represented by thick cirrus clouds, and the cover of the lower clouds can be seen well.

Comparing the output of the AWFA emission scheme in the simulation of PM_{10} particulate matter concentration at Zabol station with observational data indicated that the concentration increase trend was well simulated from April 22 to APril 24, although the model had a delay of 6 hours to predict the maximum on 24th of April. The results show that this scheme had estimated the concentration values of these particles more than the observation values (Figure 10).
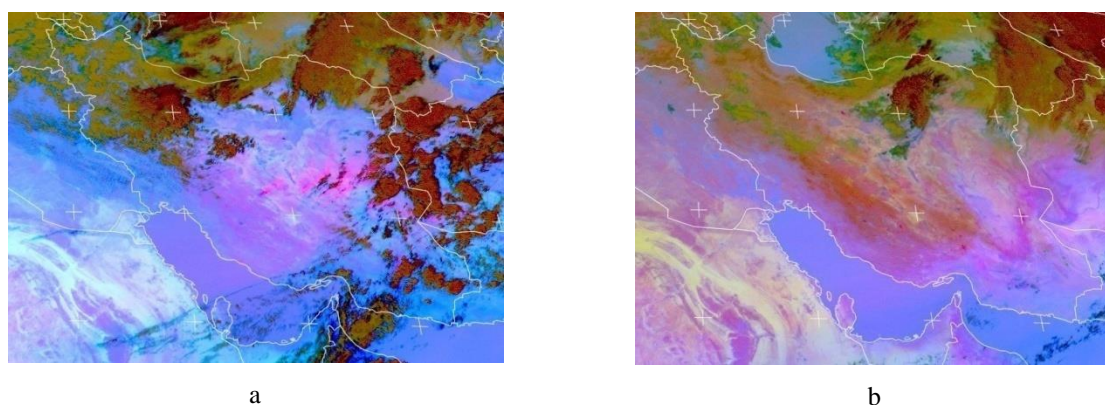
a

b

Fig. 9. RGB satellite imagery of Meteosat satellite for storms at a: 12 UTC 23, b: 12 UTC April 24, 2019.
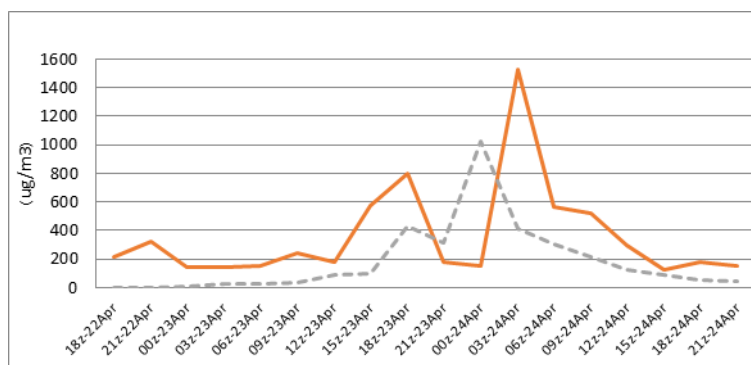
Fig. 10. PM_{10} particle concentration in (µg/m³), Zabol station on April 22, 23, and 24, 2019; and WRF-Chem output data. Dash line is observation and solid line is model output

CONCLUSION

On 23rd and 24th of April, 2019, severe dust storm and rain in many areas of the southeast, especially Kerman and Sistan and Baluchestan caused many problems. This study investigated the synoptic pattern of the region during the storm and the ability of AFWA dust emission scheme in the WRF-Chem model to simulate the dust particle concentration.

Synoptic analysis indicated the rule of strong dynamic low pressure and the passage of the front through the region. At 850 hPa level, cold and advection and baroclinicity were detected, and at the middle level of the atmosphere, a deep trough and a positive relatively vorticity were observed. Examining the vertical wind profile in the front area showed the passage of the polar jet and its penetration to lower levels. Low-level jet activity near the Lut Desert was another factor in the region's instability and the occurrence of dust storms. In general, the model output in terms of scale and time changes gave a reasonable estimate of the air vents in the study area. By producing dust particle concentration distribution maps, areas of the simulation basin with maximum particle concentration were identified as the main sources of particle emission.

Simulation of dust particles with three domains in the east of Iran, at the borders of Kerman and Sistan and Baluchestan (Fahraj and Regan) and Zabol (consecutive report code 07 of these stations) indicated that these areas were the main dust sources. In terms of agreeing with the occurrence time of severe dust phenomena, it had an acceptable agreement with the data of Zabol station. The simulated concentrations showed good validity of the temporal and spatial distribution of dust concentrations with respect to satellite RGB images and observation data. Quantitatively, the model output simulated PM_{10} particulate matter concentration values more than reality.

Examining Meteosat satellite, RGB images in the days of the storm indicated the advance of dust on the eastern and southeastern regions of Iran as well as the emergence of ridge clouds, indicating the passage of the cold front through the region. The increase in PM_{10} values as a quantity, indicating the concentration of dust particles related to Zabol station, also agreed acceptably with the model outputs. In general, not much operational and research work has been done in the eastern regions of Iran in the field of dust simulation; but the results of this study are largely consistent with the results of studies by Kargar et al., (2016).

CONFLICT OF INTEREST

The authors declare that there is not any conflict of interests regarding the publication of this manuscript. In addition, the ethical issues, including plagiarism, informed consent, misconduct, data fabrication and/or falsification, double publication and/or submission, and redundancy has been completely observed by the authors.

LIFE SCIENCE REPORTING

No life science threat was practiced in this research.

REFERENCE

Alizadeh Choobari, O., Zawar-Reza, P. and Sturman, A. (2014). The global distribution of mineral dust and its impacts on the climate system: a review. Atmos. Res., 138, 152–165. http://dx.doi.org/10.1016/j.atmosres.2013.11.007.

Chou, M. D. and Suarez, M. J. (1994). An efficient thermal infrared radiation parameterization for use in general circulation models. *NASA Tech. Memo.*, *104606*(3), p. 85.

Colarco, P., da Silva, A., Chin, M. and Diehl, T. (2009). Online simulations of global aerosol distributions in the NASA GEOS-4 model and comparisons to satellite and ground-based aerosol optical depth. J. Geophys. Res., 115, D14207. doi: 10.1029/2009JD012820.

De Longueville, F., Hountondji, Y.-C., Henry, S. and Ozer, P. (2010). What do we know about effects of desert dust on air quality and human health in West Africa compared to other regions? Science of the Total Environment. 409(1), 1-8.

Ginoux, P., Chin, M., Tegen, I., Prospero, J.M., Holben, B., Dubovik, O. and Lin, S.J. (2001). Sources and distributions of dust aerosols simulated with the GOCART model. J. Geophys. Res., 106 (D17), 20255–20273.

Goudie, A. S. (2009). Dust storms: Recent developments. Journal of environmental management, 90(1), 89-94.

Grell, G. A., Peckham, S. E., Schmitz, R., Mckeen, S.A., Frast, G., Skamarock, W. C. and Eder, B. (2005). Fully coupled "online" chemistry within the WRF model. Atmospheric Environment, 39(37), pp.6957-6975.

Grell, G. Freitas, S. R., Stuefer, M. and Fast, J. (2011). Inclusion of biomass burning in WRF-Chem: impact of wildfires on weather forecasts. Atmospheric Chemistry & Physics, 11(11).

Hong, S., Y. and Lim, O. J. (2006). The WRF single-moment microphysics scheme (WSM6). J. Korean Meteor. Soc., 42,129-151.

Iacono, M. J., Delamere, J. S., Mlawer, E. J., Shephard, M. W., Clough, S. A. and Collins, W. D. (2008). Radiative forcing by long-lived greenhouse gases: Calculations with the AER radiative transfer models, J. Geophys. Res., 113, D13103, doi: 10.1029/2008JD009944.

Karami, S., Hossein Hamzeh, N., Ranjbar Saadatabadi, A. and Mousavi, M. (2018). Synoptic study and simulation of soil storm in Khuzestan province in February 2016, Journal of Meteorology and Atmospheric Sciences, 1(2), 177-189.

Kargar, A., Bodaghjamali, J., Ranjbar Saadatabadi, A., Moineddini, M. and Goshtasb, H. (2016). Numerical simulation of sandstorms and heavy dust in eastern Iran using the WRF-Chem model (Case study: May 31 and June 1, 2011), Natural Environment, Natural Resources of Iran, 69 (4), 1077-1089.

Kawamura, R. (1951). Study on sand movement by wind, *Rep. Inst. Sci. Technol. Univ. Tokyo*, **5**(3), 95– 112.

LeGrand, S. L., Polashenski, C., Letcher, T. W., Creighton, G. A., Peckham, S. E. and Cetola, J. D. (2019). The AFWA dust emission scheme for the GOCART aerosol model in WRF-Chem v3.8.1, Geosci. Model Dev., 12, 131–166, https://doi.org/10.5194/gmd-12-131-2019.

Marticorena, B., and Bergametti, G. (1995). Modeling the atmospheric dust cycle: 1. Design of a soil-derived dust emission scheme: Journal of Geophysical Research, 100, 16415–16430, doi: 10.1029/95JD00690.

Mlawer, E. J., Taubman, S. J., Brown, P. D., Iacono, M. J. and Clough, S. A. (1997). Radiative transfer for inhomogeneous atmospheres: RRTM, a validated correlated-k model for the longwave. Journal of Geophysical Research: Atmospheres, 102(D14), 16663-16682.

Mitchell, K. (2005). The community Noah land surface model (LSM), User's Guide, available at: ftp://ftp.emc.ncep.noaa.gov/mmb/ gcp/ldas/noahlsm/ver_2.7.1 (last access: May 2018).

Nakanishi, M. and Niino, H. (2006). An Improved Mellor-Yamada Level 3 Model: Its Numerical Stability and Application to a Regional Prediction of Advection Fog. Boundary-Layer Meteorology, 119, 397-407.

Noh, Y., Cheon, W.G. and Hong, S.Y. (2003). Improvement of the K-profile model for the planetary boundary later based on Large Eddy Simulation Data. Boundary-Layer Meteorology (2003) 107: 401. https://doi.org/10.1023/A:1022146015946.

Prospero, J.M., Ginoux, P., Torres, O., Nicholson, S.E., Gill, T.E. (2002). Environmental characterization of global sources of atmospheric soil dust identified with the NIMBUS 7 Total Ozone Mapping spectrometer (TOMS) absorbing aerosol product. Rev. Geophys. 40 (1), 1002. http://dx.doi.org/ 10.1029/2000RG000095.

Ranjbar Saadatabadi, A., Mihanparast, M., Nouri, F. (2016). Study of dust phenomenon in western Iran from a meteorological perspective (long-term and short-term study), Nivar Scientific and Extension Journal, 92(93), 53-66.

Rashki, A., Kaskaoutis, D.G., Rautenbach, C. J., Eriksson, P. G., Qiang, M. and Gupta, P. (2012). Dust storms and their horizontal dust loading in the Sistan region, Iran. Aeolion Research. 5(1), 51-62.

Shao, Y. (2008). Physics and Modelling of Wind Erosion. Springer Science, New York.

Rezazadeh, M., Irannejad, P. and Shao, Y. (2013). Dust Emission Simulation with WRF-Chem Numerical Weather Prediction Model and Using New Surface Data in the Middle East: Journal of Earth and Space Physics: 39 (11), 191-212.

Squires, V.R. (2007). Dust and sandstorms: an early warning of impending disaster, P 15-25. In: Youlin, Y., V. Squires and L. Qi (Eds.), Global Alarm: Dust and Sand Storms from the World's Drylands. United Nations.

Tanaka, T. Y. and Chiba, M. (2006). A numerical study of the contributions of dust source regions to the global dust budget. Global and Planetary Change, 52(1), 88-104.

Tegen, I., Werner, M., Harrison, S. and Kohfeld, K. (2004). Relative importance of climate and land use in determining present and future global soil dust emission: Geophysical Research Letters, 31, L05105.

Thompson, G., Field, P. R., Rasmussen, R. M. and Hall, W., D. (2008). Explicit Forecasts of Winter Precipitation Using an Improved Bulk Microphysics Scheme. Part II: Implementation of a New Snow Parameterization. Mon. Wea. Rev. 136 (12): 5095–5115. https://doi.org/10.1175/2008MWR2387.1

Wang, W., Bruyère, C., Duda, M., Dudhia, J., Gill, D., Michael, K., Keene, K., Chen, M., Lin, H. C., Michalakes, J., Rizvi, S., Zhang, X., Berner, J., Soyoung, H. and Fossell, K. (2017). Guide for the Advanced Research WRF (ARW) Modeling System Version 3.9, NCAR technical note, Mesoscale and Microscale Meteorology Division, National Center for Atmospheric Research, Boulder, Colorado, USA.

Westphal, D.L., Toon, O.B. and Carlson, T.N. (1988). A case study of mobilization and transport of Saharan dust. Journal of the Atmospheric Sciences, 45(15), 2145-2175.

Westphal, D.L., Toon, O.B. and Carlson, T.N. (1987). A two-dimensional numerical investigation of the dynamics and microphysics of Saharan dust storms. Journal of Geophysical Research: Atmospheres, 92(D3), 3027-3049.

Zakey, S., Solmon, F. and Giorgi, F. (2006). Implementation and testing of a desert dust module in a regional climate model, Atmos. Chem. Phys., 6, 4687–4704.